Hydrothermal mineralization and mineral chemistry of arsenides and sulfarsenides in the Fe-Co-Ni-As-S system and introduction of three unknown minerals from the Port Radium IOCG deposit, Northwest Territories, Canada

Alireza Somarin (somarina@brandonu.ca)
Brandon University
Li Zhou
Guizhou Normal University

Research Article

Keywords: Great Bear Magmatic Zone, Port Radium, Contact Lake, Fe-Co-Ni-As-S system, sulfarsenides, mineral chemistry

Posted Date: May 3rd, 2022

DOI: https://doi.org/10.21203/rs.3.rs-1551126/v1

Abstract

The Port Radium deposit is the result of intrusion of the Mystery Island felsic-intermediate plutonic complex into the ~ 1.885 Ga supracrustal marine sedimentary rocks and volcanic suits, which formed a variety of mineralization styles from iron oxide-copper-gold (IOCG) to epithermal. Extensive and intensive hydrothermal alterations including albitic, magnetite-actinolite-apatite, potassic ± albitic, phyllic, and propylitic prepared a ground for the main sulfide, sulfarsenide and uraninite mineralization during last stage of hydrothermal activity. Scarce and weak sulfide mineralization started from the beginning of the hydrothermal activity and reached to the strongest state during epithermal stage. In addition to the common arsenides and sulfarsenides, three unknown sulfarsenides were also found: $(Co_{0.96}Ni_{0.45}Fe_{0.03})S_{0.27}As_4$ which is probably a solid solution product of cobaltite and gersdorfite; $(Ni_{2.13}Co_{0.38})S_{0.97}As_4$ and $(Ni_{1.83}Co_{0.83})S_{1.25}As_4$ which are chemically comparable to the Port Radium rammelsbergite with substantial addition of S and Co; they could also be the solid solution product of gersdorfite-cobaltite or safflorite-rammelsbergite.

Highlights

- The Port Radium U-Ag-Cu ± Ra ± Ni ± Co ± Bi deposit resulted from intrusion of the Mystery Island felsic-intermediate plutonic complex into the ~1.885 Ga sedimentary rocks and volcanic suits.
- A variety of mineralization styles from iron oxide-copper-gold (IOCG) to epithermal deposits formed in the area that are associated with extensive and intensive alterations such as albitic, magnetite-actinolite-apatite, potassic ± albitic, phyllic, and propylitic.
- Several arsenides and sulfarsenides of the Fe-Co-Ni-As-S system formed during epithermal mineralization. In addition to common known minerals of this system, three unknown sulfarsenides were also found: $(Co_{0.96}Ni_{0.45}Fe_{0.03})S_{0.27}As_4$, $(Ni_{2.13}Co_{0.38})S_{0.97}As_4$, and $(Ni_{1.83}Co_{0.83})S_{1.25}As_4$.
- The unknown sulfarsenides show extensive solid solution in cobaltite-gersdorfite and safflorite-rammelsbergite pairs of the Fe-Co-Ni-As-S system.

1. Introduction

Arsenides and sulfarsenides of the Fe-Co-Ni-As-S system form a diverse group of ore minerals that are commonly found in magmatic sulfide and hydrothermal vein deposits worldwide (e.g. Petruk et al., 1969; Hem et al., 2001; Wagner and Lorenz, 2002; Melekestseva et al., 2003; Fanlo et al., 2004, 2006; Gritsenko et al., 2004; Parviainen et al., 2008; Ahmed et al., 2009; Gervilla et al., 2012; Kiefer et al., 2017; Rezazadeh et al., 2020). Minerals of this system have been studied in experimental and field research projects for several decades (e.g. Campbell, 1955; Giese and Kerr, 1965; McWhan et al., 1972; Rajamani and Prewitt, 1973, 1975; Scott and Nowacki, 1976; Will et al., 1984; Fuess et al., 1987; Fleet and Burns, 1990; Posfai et al., 2000; Hem and Makovicky, 2004; Hem, 2006; Kiefer et al., 2017) and still going on. Each work has elucidated only part of this complicated system because there is no single ore deposit that has all possible mineral variations of this system. Polymorphism and extensive substitution of Fe-Co-Ni in the

cation site and As-S in the anion site add to the complexity of minerals in this system. Although 3 dimensional view of this system using only 3 of 5 components seems simpler, the system becomes complicated when all 5 components are considered; as a result, more knowledge gaps become visible (Hem, 2006).

The Port Radium iron oxide-copper-gold (IOCG) deposit is located in the Great Bear Magmatic Zone (GBMZ), northwestern Canada. This continental magmatic arc is part of the Wopmay orogen, which extends about 400 km and is mainly covered by felsic-intermediate volcanic rocks intruded by various granitic plutons. As a result, a wide range of mineralization styles from IOCG to porphyry, skarn and epithermal has formed (Mumin et al., 2010). Several papers have been published on the regional geology and deposit types of the area, however detailed mineralogical studies of the Port Radium deposit is still lacking. This paper describes various minerals of the Fe-Co-Ni-As-S system and their paragenesis with common ore minerals of the Port Radium deposit. In addition, micro-analytical data and compositional variation of individual minerals are presented which adds some extra light to the complicated mineralogy of the Fe-Co-Ni-As-S system. Furthermore, three unknown minerals are introduced.

2. Geological Background

Regional geology of GBMZ has been studied by several investigators and is still ongoing (e.g. Hoffman et al., 1975; Hoffman and McGlynn, 1977; Hoffman, 1980; Hildebrand, 1981, 1983; Bowring, 1984; Hildebrand et al., 1987; Goad et al., 2000a, 2000b; Gandhi et al., 2001; Mumin et al., 2007, 2010; Corriveau et al., 2010; Hildebrand et al., 2010; Montreuil et al., 2016). This zone is the result of a 1.875–1.843 Ga continental-scale felsic-intermediate Andean-type calc-alkaline magmatism in a continental magmatic arc tectonic setting near the western margin of the Archean Slave craton in northwestern Canada. This magmatic arc formed by eastward subduction-related magmatism between the 2.10–1.90 Ga arc-related Hottah terrain to the west and the pre-Great Bear Calderian accretionary wedge to the east. The products of such extensive magmatism are widespread dacite-rhyodacite-andesite volcanic and volcanoclastic sequences (~ 1.885 Ga around Port Radium) that have been intruded by granite, granodiorite, monzonite, quartz monzonite, and quartz diorite plutons. This geological setting has provided suitable conditions for a variety of mineralization styles specifically IOCG, porphyry, epithermal, and less common skarn deposits. The GBMZ hosts four best-known Canadian IOCG deposits: the NICO Co-Au-Bi and the Sue-Dianne Cu-Ag-Au deposits in southern GBMZ; Mag Hill Co-Ni-U and Port Radium Ni-Co-U-Ag in northern GBMZ (Mumin et al., 2010; Somarin and Mumin, 2014).

At Port Radium, intrusion of the quartz diorite, quartz monzonite and granite of the Mystery Island pluton into the Port Radium and Echo Bay formations developed an extensive hydrothermal system within the volcanoclastic tuff and volcanic lavas of dacite, rhyodacite and andesite composition (Fig. 1). The mineralization style is early IOCG overprinted by later epithermal veining. The Port Radium-Echo Bay district hosts past-producing Port Radium, Echo Bay, Bonanza, and El Bonanza U-Ag-Cu ± Ra ± Ni ± Co ± Bi mines which yielded > 5100 tonne Cu, > 6200 tonne U and > 907 tonne Ag. Maximum concentration for

some metals in drill cores include 9.47% Cu, 3.81% Pb, 2.93% Zn, 0.84% Ni, 2.50% Co, 1.20% U, 1.7% Bi, 2.3 ppm Au, 206 ppm Ag, and 46 ppm Th (Somarin and Mumin 2014).

3. Methodology

More than 200 samples were collected from surface and drill cores. After visual examination and petrological investigations, 50 thin-polished sections were made and studied using optical microscope at Brandon University, Canada. Ten sections with representative ore minerals were selected for further mineral-chemistry investigations using JEOL JSM-6390LV/GS scanning electron microscope equipped with an Oxford INCA X-Act energy dispersive spectrometer with acceleration voltage of 20kV and load current of 68 uA at Brandon University. Detection limit for all elements was 0.1%.

For verification and identification of some minerals, three samples were selected for X-ray diffractometry (XRD) at Brandon University. The samples were reduced to < 75 µm by crushing using a mortar and pestle and passing through a 200 mesh sieve. Fifteen milligrams of each powdered sample was inserted into 2.5mm deep steel disc holder and analyzed. Continuous scan X-ray powder-diffraction data were collected over a range 3–90° 2θ with CoKa radiation on a Rigaku Miniflex 6 diffractometer equipped with a D/tex Ultra2 detector. The fine-focus Co X-ray tube was operated at 40 kV and 0.15 mA, analyzing 10°/minute. The X-ray diffractograms were analyzed using Smartlab Studio II and the American Mineralogist Crystal Structure Database. Whole Powder Pattern Fitting method was used to further refine results and show semi-quantitative concentration of the present minerals; detection limit was 0.1%.

4. Hydrothermal Alterations

The hydrothermal alteration zone at Port Radium covers ~ 10 km^2; drilling and drill core logging indicates that this zone extends several hundreds of meters at depth. These hydrothermal alterations have a zonal pattern and vary from proximal albitic, magnetite-actinolite-apatite (MAA) at the center of the hydrothermal system to potassic ± albitic, phyllic, and peripheral/overprinted propylitic alterations. Similar alteration pattern are also found in the Mag Hill IOCG where the temperature of the hydrothermal system gradually transitioned from ~ 550°C in the center to < 150°C in the peripheral zones (Somarin and Mumin, 2014).

Albitic alteration occurs as overgrowth of the primary igneous plagioclase in the host volcanic rocks. The only sulfide mineralization at this stage is rare pyrite. Most of hydrothermal albite formed later with K-feldspar during potassic ± albitic alteration. MAA alteration is found at surface and depth of several hundreds of meters. It includes coarse grains of magnetite, dark green actinolite, and pink apatite up to several cm each grain with trace amount of pyrrhotite as disseminated grains and open space filling in the volcanic host rocks. Biotite ± fluorite locally accompany MAA alteration; biotite appears as unaltered booklets and aggregates up to a few centimeters in size; pink fluorite rarely occurs in surface samples. Textural relationships suggest that pyrrhotite formed during and after magnetite mineralization. As the

hydrothermal system evolved, magnetite content of the MAA alteration was reduced and it was gradually changed to AA (actinolite-apatite) with weak pyrrhotite-chalcopyrite-pyrite mineralization.

Following AA alteration, the potassic ± albitic alteration occurred which is commonly found at depth > 150 m. It formed K-feldspar ± albite-bearing veins, veinlets, and patchy pink color masses. In the potassic-altered rocks, K-feldspar occurs as open space filling as well as overgrowth of igneous K-feldspar. Hydrothermal albite commonly occurs as fine grains (< 0.5 mm) in the groundmass of the altered rocks. These grains are commonly replaced partially by K-feldspar suggesting that sodic alteration occurred before potassic alteration.

Quartz, sericite, and pyrite are the main products of the phyllic alteration, which occurs sporadically in the volcanic rocks as moving away from the central part of the Port Radium hydrothermal system. Replacement of igneous feldspars by sericite and overgrowth of igneous quartz are common in the phyllic-altered rocks. The main sulfide and sulfarsenide mineralization started from this stage (Fig. 2). Phyllic alteration was followed by the propylitic alteration, which formed quartz, chlorite, epidote, carbonate with trace sericite and pyrite ± chalcopyrite ± sphalerite. These minerals occur as replacement, open space filling, veins and veinlets. Replacement of hydrothermal biotite and actinolite by chlorite, and plagioclase by epidote are found locally. At depth, propylitic alteration mostly occurs as quartz-chlorite ± sulfides veins cutting MAA and potassic alterations. This alteration cuts and overlaps previous alterations and extends several kilometers away from center of the hydrothermal system. Replacement textures and cross cutting relationships show that propylitic occurred as the last alteration at Port Radium.

5. Ore Mineralization

Based on timing, intensity and extension, the Port Radium ore mineralization can be subdivided into two stages: 1) early-stage weak and limited mineralization, and 2) late-stage strong and extensive mineralization. Various ore minerals have formed during these stages (Table 1).

5.1. Early-stage ore mineralization

Although albitic, MAA and potassic alterations are intensive, widespread, and show zonal distribution, only trace ore mineralization as pyrrhotite, pyrite with trace chalcopyrite and sphalerite formed during these stages of hydrothermal activity (Fig. 2). Textural relationships suggest that pyrrhotite formed during and after magnetite mineralization in MAA (Fig. 3a). However, most of pyrrhotite formed during the AA alteration; the large pyrrhotite grains enclose euhedral apatite crystals with poiklitic texture. In addition, weak sulfide mineralization occurred at this stage and formed trace chalcopyrite and sphalerite as irregular aggregates, < 2 mm in size, accompanied by euhedral to subhedral pyrite grains. Textural and crosscutting relationships indicate that chalcopyrite, sphalerite and pyrite precipitation was mainly post-pyrrhotite mineralization.

Common opaque minerals in the potassic zone include disseminated trace magnetite, hematite, pyrrhotite and pyrite. The magnetite gradually disappeared as the system progressed towards phyllic and propylitic alterations during which oxide mineralization continued as sporadic hematite and specularite. The latter alterations mark start of the main sulfide mineralization at Port Radium, which continued later as sulfide-sulfarsenide ± uraninite epithermal mineralization.

5.2. Late-stage ore mineralization

The main sulfide mineralization started from the phyllic alteration stage. Due to high sulfide content, some phyllic zones form gossan at the surface; they range in size from a few m^2 to ~ 1 Km^2. The largest gossan is roughly parallel to vein #1 (Fig. 1) whereas the small ones are sporadic. Pyrite and trace chalcopyrite are common sulfides in the gossans. They occur as veinlets, veins, and masses up to several tens of centimeters wide and a few meters long. Pyrite and siegenite occur as skeletal and brecciated grains (Fig. 3b) up to 0.5 mm in size, hosted and replaced by chalcopyrite; brecciated pyrite grains are also cemented by chalcopyrite. Hematite and goethite replace both pyrite and chalcopyrite particularly along their fractures. Stromeyerite is rare and occurs as subhedral grains up to 15 micron associated with siegenite, and both hosted by chalcopyrite (Fig. 3b). Stromeyerite is closely associated with an Ag-Se-Te mineral, which occurs as 5–20 micron size inclusions in chalcopyrite.

The sulfide mineralization continued as pyrite-chalcopyrite ± sphalerite ± galena ± marcasite in the quartz–chlorite ± epidote veins of the propylitic alteration. These minerals commonly fill fractures and open spaces in the older MAA and potassic assemblages. These veins are still found sporadically at depth of ~ 350 m. Pyrrhotite from the earlier sulfide mineralization can be found as anhedral-subhedral grains up to 4 mm in size and locally replaced by marcasite. Pyrite occurs as anhedral grains and masses up to 2.5 cm long. Chalcopyrite occurs as inclusions and fills fractures in pyrite. Sphalerite with or without chalcopyrite inclusions is found as masses accompanied by trace galena. At shallow depth where propylitic alteration overprints potassic zone, magnetite and hematite have been obliterated whereas sulfide mineralization is enhanced locally as pyrite overgrowth and skeletal grains with trace chalcopyrite, sphalerite, galena, and pyrrhotite inclusions.

Following phyllic and propylitic alterations, the sulfide mineralization became strong and transitioned into the main ore mineralization that occurred as epithermal-type veins during late stage hydrothermal activity at Port Radium (Fig. 2). This mineralization formed 5 main ore-bearing veins that are a few meters thick and several hundreds of meters long (Fig. 1). These veins are W-NW striking with near vertical dip that show evidence of multiple hydrothermal events during episodic shearing and fracturing which extend 0.2-1 m into their immediate wall rocks. The cement of the breccia is mainly quartz ± carbonate, which occur as subhedral-euhedral grains with local growth zoning. The wall rock fragments commonly show hydrothermal alteration particularly propylitic assemblages. Uranium mineralization is mainly associated with the polymetallic sulfide and sulfarsenide veins that were historically mined for U, Cu and Ag at Port Radium. It is notable that not all sulfide and sulfarsenide veins have uraninite.

6. Sulfide Mineralization

Quartz-pyrite-chalcopyrite vein. This vein cuts the brecciated chlorite-sericite (propylitic) altered ash tuff and greywacke that are cemented by quartz. Sulfides are mainly in the vein but traces are also found in the wall rocks. Chalcopyrite occurs as masses up to several centimeters, accompanied by subhedral to euhedral pyrite grains up to 2 mm in size, trace sphalerite, and supergene chalcocite and covellite.

Quartz-carbonate-epidote-chlorite-pyrite-chalcopyrite-galena-sphalerite assemblage. This epithermal sulfide mineralization is cotemporaneous with propylitic alteration that overprints MAA alteration. The assemblage occurs as irregular masses or veins up to a few cm thick. Locally anhedral to subhedral grains of epidote up to 1 cm in size, comprise 85 vol% of the veins. Potassium feldspar (possibly adularia) occurs sporadically along the vein walls and infiltrates into the host rock. Galena occurs as individual grains associated with chalcopyrite or as replacement of pyrite. Marcasite is common and replaces pyrite(?) and pyrrhotite. Commonly, galena, sphalerite, and chalcopyrite fill fractures in pyrite. Some sphalerite grains host chalcopyrite inclusions; based on optical features, most sphalerite grains are Fe-poor. Locally, chalcopyrite is rimmed by galena which itself is rimmed by sphalerite indicating that chalcopyrite is paragenetically older. Sphalerite ± galena ± chalcopyrite fill fractures in, and replace, pyrrhotite and pyrite indicating that pyrrhotite ± pyrite (formed during MAA alteration) are the oldest sulfides at Port Radium. This agrees with general paragenetic sequence of the Port Radium deposit, which is similar to that at Mag Hill (Somarin and Mumin, 2014).

7. Sulfarsenide Mineralization

Quartz-carbonate-cobaltite-skutterudite-pyrite-chalcopyrite ± sphalerite ± arsenopyrite assemblage. This assemblage is a part of vein #3 at Port Radium. The exposed part of the vein is 0.2–1.5 m wide and several hundred meters long. The andesitic wall rock shows phyllic alteration and it is brecciated near the vein wall. Quartz and euhedral dolomite occur as coarse grains up to 6 mm (Fig. 3c). Cobaltite occurs as subhedral to euhedral grains up to 1 mm in size accompanied by zoned skutterudite up to 3 mm in size (Fig. 3d). Two types of Co mineralization are found in this vein: 1) cobaltite- skutterudite in the intensely altered and brecciated wall rock fragments that are cemented by quartz and calcite; 2) cobaltite-skutterudite as coarser grains filling open spaces in the vein (Fig. 3e).

Similar assemblage also occurs as part of vein #1 that cuts intensely brecciated Port Radium Formation with chlorite-carbonate (propylitic) alteration. In this vein, chalcopyrite occurs as massive aggregates up to a few 10s of cm in size, containing inclusions of other sulfides. Millimeter-centimeter scale sphalerite with or without chalcopyrite inclusions accompanies chalcopyrite masses. Arsenopyrite as < 2 mm euhedral grains fills spaces between chalcopyrite and sphalerite grains, or occurs as inclusions inside them. Subhedral-anhedral pyrite grains, < 3 mm in size, have been brecciated and cemented by chalcopyrite and arsenobismuthian tetrahedrite (Fig. 3f).

Quartz- niccolite-cobaltite vein. This assemblage is a part of vein #1 and represents Ni-Co arsenide mineralization at Port Radium. Both niccolite and rammelsbergite are the main arsenides associated with cobaltite and form masses up to a few tens of centimeters. Rammelsbergite fills fractures in niccolite. Gersdorffite occurs as subhedral grains in the contact of niccolite and rammelsbergite (Fig. 3g). It appears that gersdorfite is the reaction product of rammelsbergite with S-bearing solution.

8. Uranium-sulfide-sulfarsenide Mineralization

Quartz-uraninite-chalcopyrite-pyrite ± cobaltite ± arsenopyrite ± tetrahedrite assemblage. This assemblage is a part of vein #1 that was one of the main veins mined at Port Radium. Although this vein has a polymetallic assemblage, not all ore minerals have formed at the same time. Quartz occurs as anhedral to subhedral grains up to 1.2 cm long. Uraninite is the main ore mineral in this assemblage and occurs as colloform and botryoidal masses, up to a few centimeters in size. Some colloform uraninite masses have quartz as nucleolus (Fig. 3h). These masses locally cut quartz-pyrite-chalcopyrite ± galena ± tetrahedrite ± arsenopyrite veinlets; all sulfides in the veinlets are trace. Cobaltite and arsenopyrite occur as subhedral-euhedral crystals up to 0.5 mm. Tetrahedrite is anhedral, up to 0.25 mm in size, and commonly accompanies chalcopyrite. Galena and trace coffinite (verified by XRD) as decay and alteration products of uraninite, respectively, accompany and fill fractures in uraninite (Fig. 3i). Uranophane is also found in the weathered samples.

Quartz-carbonate-pyrite-chalcopyrite-cobaltite-skutterudite-rammelsbergite-aikinite- emplectite-native bismuth-uraninite assemblage. This assemblage is also part of vein # 1. Although the hand specimen does not contain visible uraninite, U mineralization has been observed in other parts of this vein. The wall rock shows intense brecciation where chlorite-epidote-carbonate (propylitic) altered country rocks have been cemented by carbonate. Chalcopyrite and pyrite occur as trace disseminated grains and aggregates, up to 5 mm in size, where locally chalcopyrite fills fractures in pyrite. Aikinite rims sphalerite and chalcopyrite (Fig. 4a) suggesting it formed after base metal sulfides. Also aikinite occurs as subhedral grains up to 0.3 mm in size with poiklitic texture associated with native bismuth, emplectite, and Ni-Co sulfide/sulfarsenides (Fig. 4b, c). Cobaltite and skutterudite form rhythmic bands; cobaltite bands have clear color compared to the skutterudite bands (Fig. 4b). Skutterudite grains, up to 3 mm, are commonly zoned (Fig. 4d). Concentric bands of safflorite are commonly rimmed by cobaltite and skutterudite (Fig. 4e). An unknown mineral (called unknown 1 herein) with growth zoning, white color with faint creamy tint in polarized light, without pleochroism, and isotropic or weakly anisotropic is associated with Ni-Co sulfarsenides (Fig. 4c, d). This mineral has optical properties similar to skutterudite however its chemistry is different (see below). In addition, there is another unknown mineral (called unknown 2 herein) with concentric bands, creamy white color in polarized light, without pleochroism and strongly anisotropic (Fig. 4e). Optically, this mineral is similar to rammelsbergite but their chemistry is different (see below). The third unknown mineral (unknown 3) is less common, closely associated with rammelsbergite and optically similar to unknown 2.

Native bismuth rims safflorite and fills cracks in cobaltite (Fig. 4f). Emplectite occurs as fine inclusions up to 50 micron associated with aikinite (Fig. 4c). Erythrite and heterogenite (verified by XRD) are common weathering products of cobaltite.

In this assemblage, quartz grains are up to 1 cm long with growth zoning. Dolomite occurs as open space filling. Where this vein cuts MAA zone, magnetite is hematitized along grain boundaries/margins, and chlorite-calcite-quartz occurs as pseudomorph after actinolite.

9. Mineral Chemistry

Pyrrhotite has up to 0.81% Ni and 0.35% Co (Table 2). Pyrite grains have higher Ni (up to 2.09%) and Co (up to 0.48%) than pyrrhotite. Marcasite has similar Co (up to 0.50%) but more Ni (up to 5.02%) than pyrite (Table 2). These elements are likely substitute Fe in the structure of these minerals. Some arsenopyrite grains have traces of Co, Ni, Cu, Sb (Table 2). Chalcopyrite has up to 0.39% Sb and 0.36% Co (Table 2).

Sphalerite grains without chalcopyrite inclusions have wide range of Cu from below detection limit to 5.02%, whereas Cu range is narrow (0.45–1.07%) in sphalerite grains with chalcopyrite inclusions. Similarly, chalcopyrite-free sphalerite has wider Fe content (0.58–4.76%) compared to the chalcopyrite-bearing sphalerite (1.46–2.23%). Overall Fe content is low which reflects light color of the Port Radium sphalerite (Table 3). Galena contains up to 0.64% Ag and 2.7% Zn (Table 3). Native bismuth have traces of As (up to 0.4%) and Ag (0.58% in one sample).

The Port Radium tetrahedrite is enriched in As and Bi (up to 6.85% and 8.27%, respectively; Table 4). Emplectite is relatively rare and has up to 0.23% Co, 0.35% Ni and 0.72% Sb. Aikinite contains up to 0.39% Ag, 0.60% Fe, 0.40% Ni, and 0.31% Co (Table 4)

Most of microanalysis of stromeyerite did not produce reliable results due to its small size and beam overlap with the host chalcopyrite. One relatively larger grain produced a reliable data with 1.02% Fe (Table 5). Stromeyerite is closely associated with an Ag-Se-Te mineral with a tentative formula of $(FeCu)_{0.82}Ag_{4.03}Se_{2.00}S_{0.30}Te_{0.16}$ which could be a Te-bearing aquilarite (Ag_4SeS) or naumannite (Ag_2Se) with some Fe-Cu-S input from the host chalcopyrite.
The Port Radium uraninite is characterized by UO_2 range of 76.77–86.70% (average 84.18%) and high PbO (9.90-22.37% with an average of 13.67%) (Table 6). The lead has negative correlation with UO_2 showing that it is decay product of uranium (Fig. 5a). The high Pb content is similar to the Eagle Point, Macarthur River and Camie River deposits, Canada (Alexandre et al., 2016). ZrO_2 reaches up to 2.43% and has preserved its initial substitution trend with uranium (Fig. 5b). SiO_2 and FeO which form during alteration of uraninite (Fig. 5c), are low (average 0.77% and 0.26%, respectively). There is no chemical difference between colloform and other forms of uraninite. The uraninite is replaced by coffinite along fractures. Coffinite composition shows a wider range (Table 6) which depends on the completeness of the replacement.

10. Fe-co-ni-as-s System

The only Ni-Co sulfide found in this research is siegenite which has up to 0.63% Cu and 4.21% Fe (Table 7) with analytical formula of $(Ni_{1.37}Co_{1.69}Fe_{0.13})S_4$. Niccolite and rammelsbergite have up to 0.82 and 3.04% Co with formulas of $Ni_{0.99}As$ and $Ni_{1.01}Co_{0.04}S_{0.09}As_2$, respectively (Table 7); the latter has also up to 0.31% Sb (Table 7). Gersdorfite ($Ni_{0.87}Co_{0.02}AsS_{0.83}$) generally has <0.5% Co (except in one sample with 3.44% Co; Table 7); one sample has 12.38% Co with a formula of $Ni_{0.64}Co_{0.37}Fe_{0.08}AsS_{1.08}$ which is called cobaltoan gersdorfite herein. Common safflorite has up to 1.2% Ni with formula of $(Co_{0.92}Ni_{0.02}Fe_{0.09})S_{0.06}As_2$ (Table 8); however some safflorite has 3.52-6.14% Ni which yields a formula of $(Co_{0.78}Ni_{0.19}Fe_{0.11})S_{0.08}As_2$ which is called nickeliferous safflorite herein. Optical properties of nickeliferous safflorite and cobaltoan gersdorfite are the same as safflorite and gersdorfite, respectively.

Skutterudite has low Ni (0.25-0.35%) but high S (4.30-8.42%) which yields a formula of $(Co_{1.01}Fe_{0.25}Ni_{0.01})S_{0.54}As_2$. The Port Radium cobaltite has 0.9-6.44% Fe and 5.37-8.94% Ni with a formula of $(Co_{0.72}Fe_{0.06}Ni_{0.14})S_{0.85}As$ (Table 9); traces of Cu and Sb are also found in cobaltite.

In addition to the known minerals of the Fe-Co-Ni-As-S system, three unknown minerals are also identified: unknown 1 $(Co_{0.96}Ni_{0.45}Fe_{0.03})S_{0.27}As_4$, unknown 2 $(Ni_{2.13}Co_{0.38})S_{0.97}As_4$, and unknown 3 $(Ni_{1.83}Co_{0.83})S_{1.25}As_4$ (Table 10). These three minerals plot on separate fields in the Co-As-S, Ni-As-S, and As-Ni-Co diagrams (Fig. 6). In the As/S vs. Ni/Co plot, these unknown sulfarsenides plot on discrete fields in the central part of the graph (Fig. 7).

11. Discussion

The GBMZ has experienced a prolonged arc-related magmatism that intruded felsic-intermediate plutonic bodies into the ~1.885 Ga Echo Bay and Port Radium supracrustal marine sedimentary rocks and volcanic suits. This magmatism created a perfect geological environment for the formation of a variety of ore deposits and introduced a substantial amount of metals such as Fe, Cu, Pb, Zn, Ni, Co, U, Bi, and somewhat Au, Ag, and Th. The Richardson high heat production pluton located 9 km south of Port Radium (Fig. 1) is enriched in some of these metals (particularly U and Th) and may have partially been the source of some of these metals (Somarin and Mumin, 2012).

The main ore mineralization of the Port Radium deposit occurred during epithermal veining which followed an extensive and intensive IOCG-style hydrothermal alterations including albitic, MAA, potassic, phyllic and propylitic. It appears that occurrence of phyllic-propylitic alterations before epithermal veining is a common feature in IOCG deposits of Port Radium and other IOCG deposits of the GBMZ (Somarin and Mumin, 2014; Klapheke, 2018). Various types of veins and hydrothermal assemblages formed during fluid-rock interactions and evolution of the Port Radium hydrothermal system. These complex textural and compositional variations in the ore mineralogy reflect rapid changes in temperature and chemical activities in the system (Somarin and Mumin, 2014).

Although sulfide mineralization is younger than MAA alteration, drill core logging and drill assay data of IOCG-style deposits in GBMZ (Somarin and Mumin, 2008; Somarin and Mumin, 2014; Klapheke, 2018) indicate that MAA zones always have high base metal concentrations. This may suggest that either both MAA and sulfide mineralizations utilized the same channels for precipitation, or MAA prepared the ground for sulfide mineralization by alteration of the country rocks which were subsequently fractured easily forming channels for movement of the base metal-bearing hydrothermal solution. As the hydrothermal system evolved, magnetite content of the MAA alteration was reduced and sulfide mineralization progressed. This manifests as MAA transitioning into AA-pyrrhotite-pyrite-chalcopyrite reflecting changing in the fugacity of oxygen and sulfur in the hydrothermal system.

Sulfide and sulfarsenide mineralization in the strongly altered wall rocks occurred possibly due to reaction of the hydrothermal solution with the country rocks. Such reactions commonly formed fine-grained hydrothermal assemblages at Port Radium (Fig. 3e). In contrast, similar minerals precipitated as coarser grains in the veins due to boiling or sudden changes in the pressure and temperature of the hydrothermal fluid (Somarin and Mumin, 2014). Intense brecciation of the wall rocks of the veins suggests high fluid pressure during hydrothermal activity that caused hydrofracturing of the surrounding rocks. Propylitic alteration of the wall rock fragments shows that main ore mineralization of Port Radium occurred after propylitic alteration. The cross cutting relationship and textural features show that uranium mineralization occurred almost simultaneously with sulfides and sulfarsenide mineralization in veins and continued after them, probably suggesting change in the oxidation state of the system. This temporal and spatial relationship between U and sulfides-sulfarsenide mineralization can be used as an exploration tool for uranium mineralization.

As the Port Radium hydrothermal system was enriched in Ni-Co, not only the common sulfides (e.g. pyrite and pyrrhotite) but also others such as sphalerite, chalcopyrite, arsenopyrite, tetrahedrite, emplectite, and aikinite have traces of these metals (as substitutes for Fe and possibly Zn and Cu).

Safflorite, gersdorfite, skutterudite, cobaltite, niccolite, and rammelsbergite are common minerals of the Fe-Co-Ni-As-S system that are found at Port Radium. Three unknown minerals with $(Co_{0.96}Ni_{0.45}Fe_{0.03})S_{0.27}As_4$, $(Ni_{2.13}Co_{0.38})S_{0.97}As_4$, and $(Ni_{1.83}Co_{0.83})S_{1.25}As_4$ formulas are also found that show distinct compositional differences with known minerals of this system (Figs. 6, 7). The nomenclature guidelines of International Mineral Association (IMA) states that in a continuous solid solution, only end members are considered as species (Nickel and Grice, 1998). For example, if a mineral has at least 50 mole% of an end member, it is named after that end member. This rule is easily applicable to continuous solid solutions where the end members have similar structures; its application becomes complicated in minerals with complex structures and multiple substitutions (Nickel and Grice, 1998; Kiefer et al., 2017). Mineral unknown 1 $(Co_{0.96}Ni_{0.45}Fe_{0.03})S_{0.27}As_4$ is possibly a solid solution product of cobaltite and gersdorfite. The resulted mineral is chemically and optically different than both cobaltite and gersdorfite.

Mineral unknown 2 $(Ni_{2.13}Co_{0.38})S_{0.97}As_4$ and unknown 3 $(Ni_{1.83}Co_{0.83})S_{1.25}As_4$ are chemically comparable to the Port Radium rammelsbergite ($Ni_{1.01}Co_{0.04}S_{0.09}As_2$ or $Ni_{2.02}Co_{0.08}S_{0.18}As_4$) with substantial addition of S and Co. Similarly, addition of S to rammelsbergite by hydrothermal solution and formation of gersdorfite has already been documented at Port Radium (Fig. 3g). It is notable that the added S and Co did not substantially replace As and Ni, respectively, as apfu values of As and Ni are similar in these unknown minerals and rammelsbergite. Mineral unknown 2 and unknown 3 could also be a solid solution product of gersdorfite-cobaltite or safflorite-rammelsbergite (Hem, 2006). The addition or vast substitution of As-S and Ni-Co-Fe in the Fe-Co-Ni-As-S system changes unit cells and form different minerals (Hem, 2006). These changes may affect optical properties including anisotropism of the sulfarsenide (Kiefer et al., 2017).

12. Conclusions

Intrusion of the felsic-intermediate plutons into the Echo Bay and Port Radium sedimentary rocks and syn-volcanic sequences developed a classic IOCG hydrothermal system at Port Radium. This caused a variety of hydrothermal alterations from albitic to MAA, potassic ± albitic, phyllic, and propylitic. Weak sulfide mineralization started from the beginning of the hydrothermal activity and became very strong during late stage epithermal mineralization when various arsenide/sulfarsenide minerals formed with or without uraninite. Unknown sulfarsenide mineral 1 with $(Co_{0.96}Ni_{0.45}Fe_{0.03})S_{0.27}As_4$ formula is possibly a cobaltite-gersdorfite solid solution. Mineral unknown 2 $(Ni_{2.13}Co_{0.38})S_{0.97}As_4$ and unknown 3 $(Ni_{1.83}Co_{0.83})S_{1.25}As_4$ could be a solid solution of gersdorfite-cobaltite or safflorite-rammelsbergite. These indicate that the Fe-Co-Ni-As-S system is complex and more minerals naturally form in this system.

Declarations

Acknowledgment

This work was funded by the National Natural Science Foundation of China (92162219), Chinese Academy of Sciences President's International Fellowship Initiative (Grant No. 2020VCA0003), and BURC grant from the Brandon University, Canada. The manuscript benefitted greatly from comments and critical review of anonymous reviewers.

Funding: This research was funded by National Natural Science Foundation of China (92162219), Chinese Academy of Sciences President's International Fellowship Initiative (Grant No. 2020VCA0003), and BURC grant from the Brandon University, Canada.

Data availability: All data are included in this manuscript. No other data are available.

Author Contributions: Both authors contributed to the study conception and design. Alireza Somarin did field work, sample preparation, analyses, writing, and interpretations. Li Zhou contributed to sample analysis and interpretation. The first draft of the manuscript was written by Alireza Somarin and both

authors commented on previous versions of the manuscript. Both authors read and approved the final manuscript.

Competing Interests: The authors declare no conflicts of interest.

Ethical Approval: The study did not require ethical approval.

Consent to Publish: You have our permission to publish the work after due process.

Consent to Participate: This material is the authors' own original work, which has not been previously published elsewhere. All sources used are properly disclosed.

References

1. Ahmed AH, Arai S, Ikenne M (2009) Mineralogy and paragenesis of the Co-Ni arsenide ores of BouAzzer, Anti-Atlas, Morocco. Econ Geol 104:249–266
2. Bowring SA (1984) U-Pb zircon geochronology of Early Protrozoic Wopmay Orogen, N.W.T., Canada: an example of rapid crustal evolution. Unpublished PhD thesis, University of Kansas, Lawrence, 148 p
3. Campbell DD (1955) Geology of the pitchblende deposits of Port Radium, Great Bear Lake, N.W.T. Dissertation (Ph.D.), California Institute of Technology. doi:10.7907/6BX5-4F69
4. Corriveau L, Williams PJ, Mumin AH (2010) Alteration vectors to IOCG mineralization: from uncharted terranes to deposits. In: Corriveau, L., Mumin, A.H. (Eds.), Exploring for Iron Oxide Copper-Gold Deposits: Canada and Global Analogues. Geological Association of Canada, Short Course Notes, 20, 89–110
5. Fanlo I, Subías I, Gervilla F, Paniagua A, García B (2004) The composition of Co–Ni–Fe sulfarsenides, diarsenides and triarsenides from the San Juan de Plan deposit, central Pyrenees, Spain. Can Mineral 42:1221–1240
6. Fleet ME, Burns PC (1990) Structure and twinning of cobaltite. Can Mineral 28:719–723
7. Fuess H, Kratz T, Toepel-Schadt J, Miehe G (1987) Crystal structure refinement and electron microscopy of arsenopyrite. Z Kristallogr 179:335–346
8. Gandhi SS, Mortensen JK, Prasad N, van Breemen O (2001) Magmatic evolution of the southern Great Bear continental arc, northwestern Canadian Shield: Geochronological constraints. Can J Earth Sci 38:767–785
9. Gervilla F, Fanlo I, Colás V, Subías I (2012) Mineral compositions and phase relations of Ni-Co-Fe arsenide ores from the Aghbar Mine, Bou Azzer, Marocco. Can Mineral 50:447–470
10. Giese RF, Kerr PF (1965) The crystal structures of ordered and disordered cobaltite. Am Mineral 50:1002–1014
11. Goad RE, Mumin AH, Duke NA, Neale KL, Mulligan DL (2000a) Geology of the Proterozoic iron oxide-hosted NICO cobalt-gold-bismuth, and Sue Dianne copper-silver deposits, southern Great Bear

Magmatic Zone, Northwest Territories, Canada. In: Porter, T.M. (Ed.), Hydrothermal iron oxide copper-gold and related deposits: A global perspective. Australian Mineral Foundation, 1, 249–267

12. Goad RE, Mumin AH, Duke NA, Neale KL, Mulligan DL, Camier WJ (2000b) The NICO and Sue-Dianne Proterozoic, iron oxide-hosted, polymetallic deposits, Northwest Territories: application of the Olympic Dam model in exploration. Explor Min Geol 9:123–140
13. Gritsenko YD, Spiridonov EM, Vinogradova RA (2004) New data on diarsenides of the löllingite–rammelsbergite series. Dokl. Earth Sci., 399 A, 1264–1267
14. Hem SR (2006) Solid solutions in the Fe–Co–Ni–As–S system. Chem Geol 225:291–303
15. Hem SR, Makovicky E (2004) The system Fe–Co–Ni–As–S. II. Phase relations in the (Fe Co, Ni)$As_{1.5}S_{0.5}$ section at 650° and 500°C. Can Mineral 42:63–86
16. Hem SR, Makovicky E, Gervilla F (2001) Compositional trends in Fe, Co and Ni sulfarsenides and their crystal-chemical implications: results from the Arroyo de la Cueva deposits, Ronda peridotite, Southern Spain. Can Mineral 39:831–853
17. Hildebrand RS (1981) Early Proterozoic LaBine Group of Wopmay orogen: remnant of a continental volcanic arc developed during oblique convergence. In: Campbell, F.H.A. (Ed.), Proterozoic Basins in Canada. Geological Survey of Canada Paper, 81, 133–156
18. Hildebrand RS (1983) Geology of the Echo Bay-MacAlpine Channel area, District of Mackenzie. Geological Survey of Canada, Map 1546A, scale 1:50,000
19. Hildebrand RS, Hoffman PF, Bowring SA (1987) Tectonomagmatic evolution of the 1.9 Ga Great Bear magmatic zone, Wopmay orogen, northwestern Canada. J Volcanol Geoth Res 32:99–118
20. Hildebrand RS, Hoffman PF, Bowring SA (2010) The Calderian orogeny in Wopmay orogen (1.9 Ga), northwestern Canadian Shield. Geol Soc Am Bull 122:794–814
21. Hoffman PF (1980) Wopmay orogen: A Wilson cycle of early Proterozoic age in the northwest of the Canadian Shield. In: Strangway, D.W. (Ed.), The Continental Crust and its Mineral Deposits. Geological Association of Canada Special Paper, 20, 523–549
22. Hoffman PF, Bell I, Tirrul R (1975) Volcanism and plutonism, Sloan River map-area (86K), Great Bear Lake, District of Mackenzie. In Report of Activities, Part A, Geological Survey of Canada Paper, 75-1A, 331–337
23. Hoffman PF, McGlynn JC (1977) Great Bear Batholith: A volcano-plutonic depression. In Baragar, W.R.A., Coleman, L.C., Hall, J.M. (Eds.), Volcanic Regimes in Canada. Geological Association of Canada Special Paper, 16, 170–192
24. Kiefer S, Majzlan J, Chovan M, Stevko M (2017) Mineral compositions and phase relations of the complex sulfarsenides and arsenides from Dobsina (Western Carpathians, Slovakia). Ore Geol Rev 89:894–908
25. Klapheke M (2019) Comparison of the K2 IOCG-type deposit, Great Bear Magmatic Zone, NWT, with the Carmax Cu-Mo porphyry deposit, BC. Unpublished MSc thesis, Brandon University, 164p

26. McWhan DB, Marezio M, Remeika JP, Dernier PD (1972) Pressure–temperature phase diagram and crystal structure of NiS. Phys Rev Ser 3 B 5:2552–2555
27. Melekestseva IY, Zaikov VV, Tesalina SG (2003) Sulfoarsenides and arsenides of Co, Fe and Ni in ores of Ishkininsk cobalt-copper massive sulfide deposit of southern Urals. Zapiski Vserossiiskogo Mineralogicheskogo Obshchestva 132:66–77
28. Montreuil JF, Corriveau L, Davis WJ (2016) Tectonomagmatic Evolution of the Southern Great Bear Magmatic Zone (Northwest Territories, Canada): Implications for the Genesis of Iron Oxide-Alkali–Altered Hydrothermal Systems. Econ Geol 111:2111–2138
29. Mumin AH, Corriveau L, Somarin AK, Ootes L (2007) IOCG-type polymetallic mineralization in the Contact Lake Belt, Great Bear Magmatic Zone, Northwest Territories. Explor Min Geol 16:187–208
30. Mumin AH, Somarin AK, Jones B, Corriveau L, Ootes L, Camier J (2010) The IOCG-porphyry-epithermal continuum in the Great Bear Magmatic Zone, Northwest Territories, Canada. In: Corriveau, L., Mumin, A.H. (Eds.), Exploring for Iron Oxide Copper-Gold Deposits: Canada and Global Analogues. Geological Association of Canada, GAC SCN, 20, 59–78
31. Nickel E, Grice JD (1998) The IMA Commission on New Minerals and Mineral Names: procedures and guidelines on mineral nomenclature, 1998. Mineral Petrol 64:237–263
32. Parviainen A, Gervilla F, Melgarejo JC, Johanson B (2008) Low-temperature, platinum-group elements-bearing Ni arsenide assemblage from the Atrevida mine (Catalonian Coastal Ranges, NE Spain). Neues Jb Miner Abh 185:33–49
33. Petruk W, Harris DC, Stewart JM (1969) Langisite, a new mineral, and the rare minerals cobalt pentlandite, siegenite, parkerite and bravoite from the Langis mine, Cobalt-Gowganda area, Ontario. Can Mineral 9:597–616
34. Posfai M, Sharp TG, Kontny A (2000) Pyrrhotite varieties from the 9.1 km deep borehole of the KTB project. Am Mineral 85:1406–1415
35. Rajamani V, Prewitt CT (1973) Crystal chemistry of natural pentlandites. Can Mineral 12:178–187
36. Rezazadeh S, Hosseinzadeh MR, Raith JG, Moayyed M (2020) Mineral chemistry and phase relations of Co–Ni arsenides and sulfarsenides from the Baycheh-Bagh deposit, Zanjan province, Iran. Ore Geol Rev 127. https://doi.org/10.1016/j.oregeorev.2020.103836
37. Scott JD, Nowacki W (1976) The crystal structure of alloclasite, CoAsS, and the alloclasite–cobaltite transformation. Can Mineral 14:561–566
38. Somarin AK, Mumin AH (2008) Geochemistry and possible source of metals and alkalies for the Port Radium IOCG style hydrothermal system, Great Bear Magmatic Zone, Northwest Territories, Canada. Geological Association of Canada and Mineralogical Association of Canada Annual Meeting, Quebec City, Quebec
39. Somarin AK, Mumin AH (2012) The Paleo-Proterozoic high heat production Richardson Granite, Great Bear Magmatic Zone, Northwest Territories, Canada: Source of U for Port Radium? Resour Geol 62:227–242

40. Somarin AK, Mumin AH (2014) P-T-composition and evolution of paleofluids in the Precambrian Mag Hill volcano-plutonic system, Northwest Territories, Canada. Miner Deposita 49:199–215
41. Wagner T, Lorenz J (2002) Mineralogy of complex Co–Ni–Bi vein mineralization, Bieber deposit. Spessart Ger Mineralogical Magazine 66:385–407
42. Will G, Lauterjung J, Schmitz H, Hinze E (1984) The bulk moduli of 3d-transition element pyrites measured with synchrotron radiation in a new belt type apparatus. Mater. Res. Soc. Symp. Proc., 22, 49– 52

Tables

Table 1-10 are available in the Supplemental Files section.

Figures

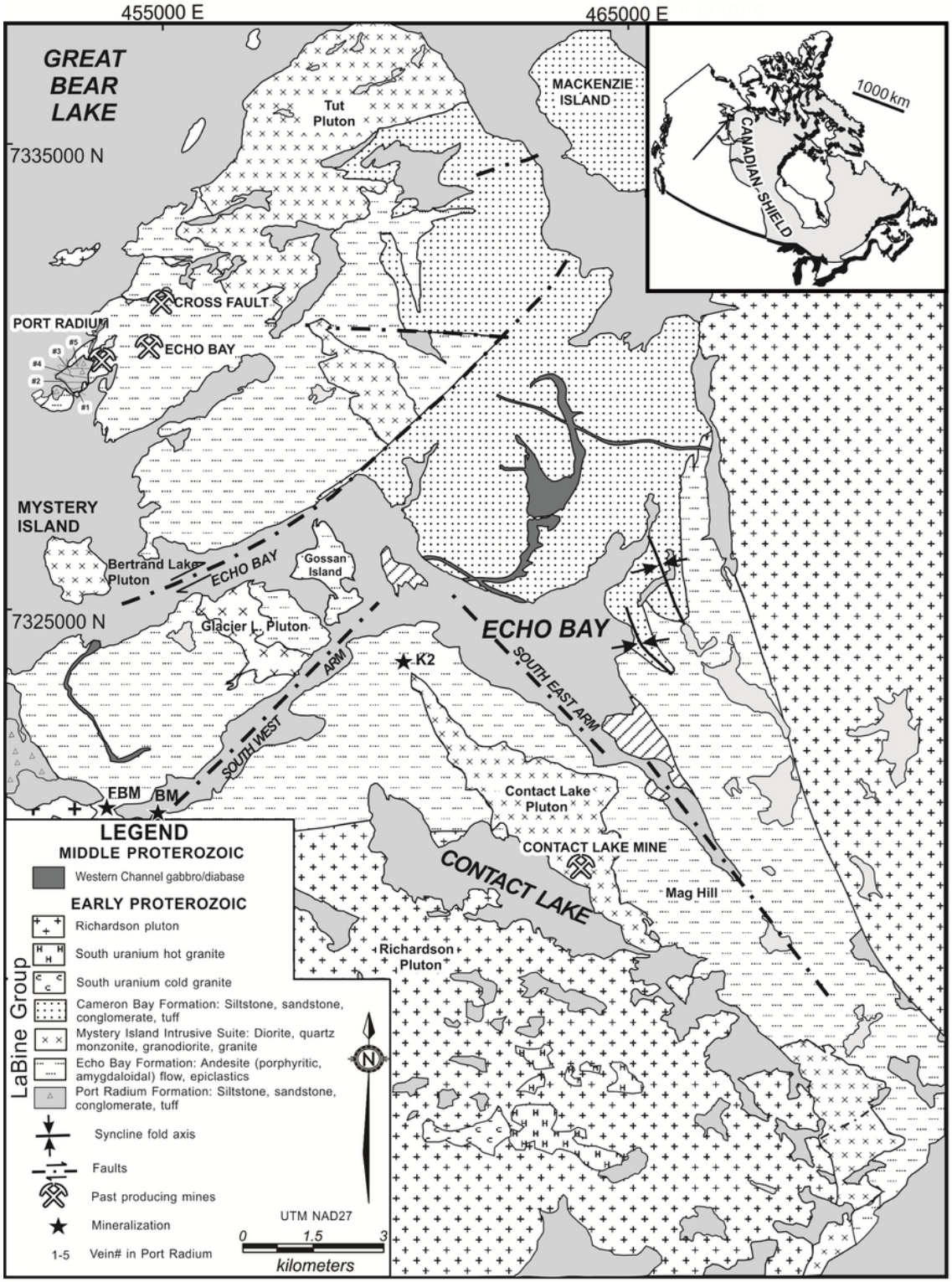

Figure 1

Regional geology map of the GBMZ (modified after Somarin and Mumin 2014).

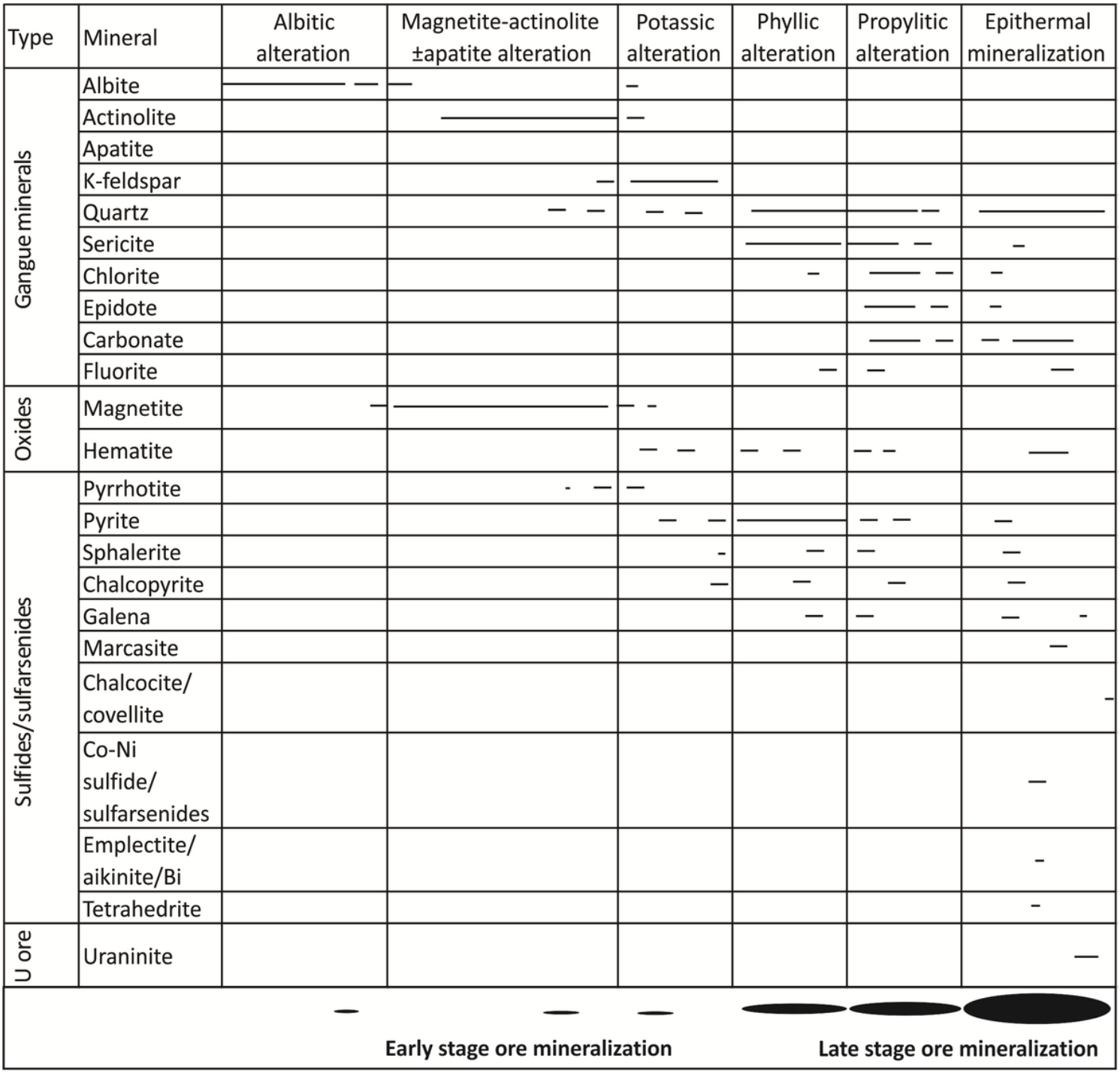

Figure 2

Paragenesis of ore and gangue minerals of Port Radium.

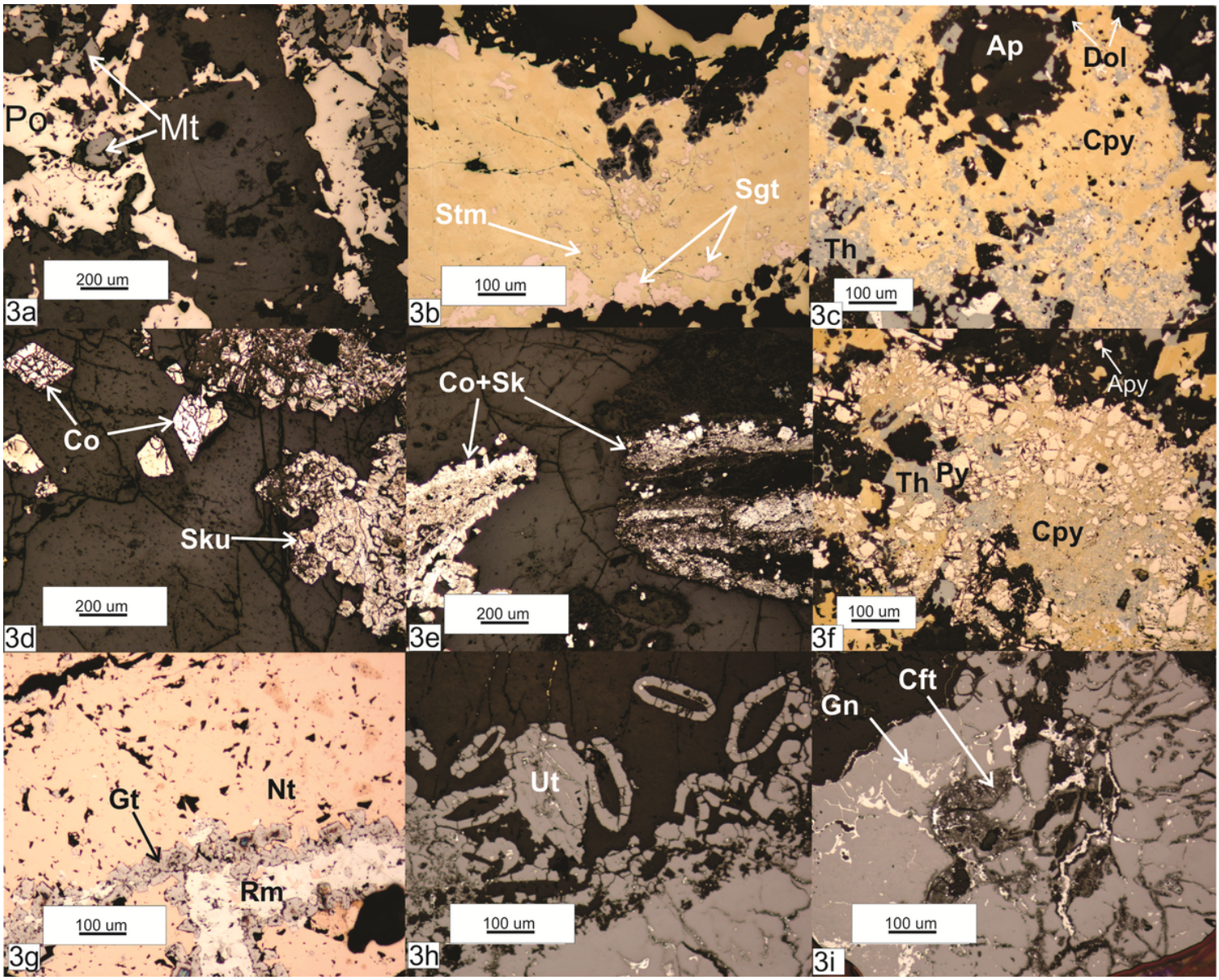

Figure 3

a) Pyrrhotite and magnetite in MAA. b) Siegenite brecciated and replaced by chalcopyrite. Stromeyerite inclusions are disseminated inside chalcopyrite. c) Apatite from MAA overprinted by epithermal mineralization including chalcopyrite hosting euhedral dolomite and arsenopyrite, fine anhedral pyrite and tetrahedrite. d) Subhedral-euhedral cobaltite accompanied by zoned skutterudite. e) Fine-grained cobaltite- skutterudite in the brecciated wall rock fragments (right side) along with coarse-grained open space filling cobaltite-skutterudite in the vein (left side). f) Subhedral-anhedral pyrite grains brecciated and cemented by chalcopyrite and arsenobismuthian tetrahedrite. g) Niccolite cut by a veinlet of rammelsbergite; gersdorfite occurs between these two minerals. h) Colloform uraninite with quartz nucleus. i) Galena and trace coffinite as decay and alteration products of uraninite, respectively.

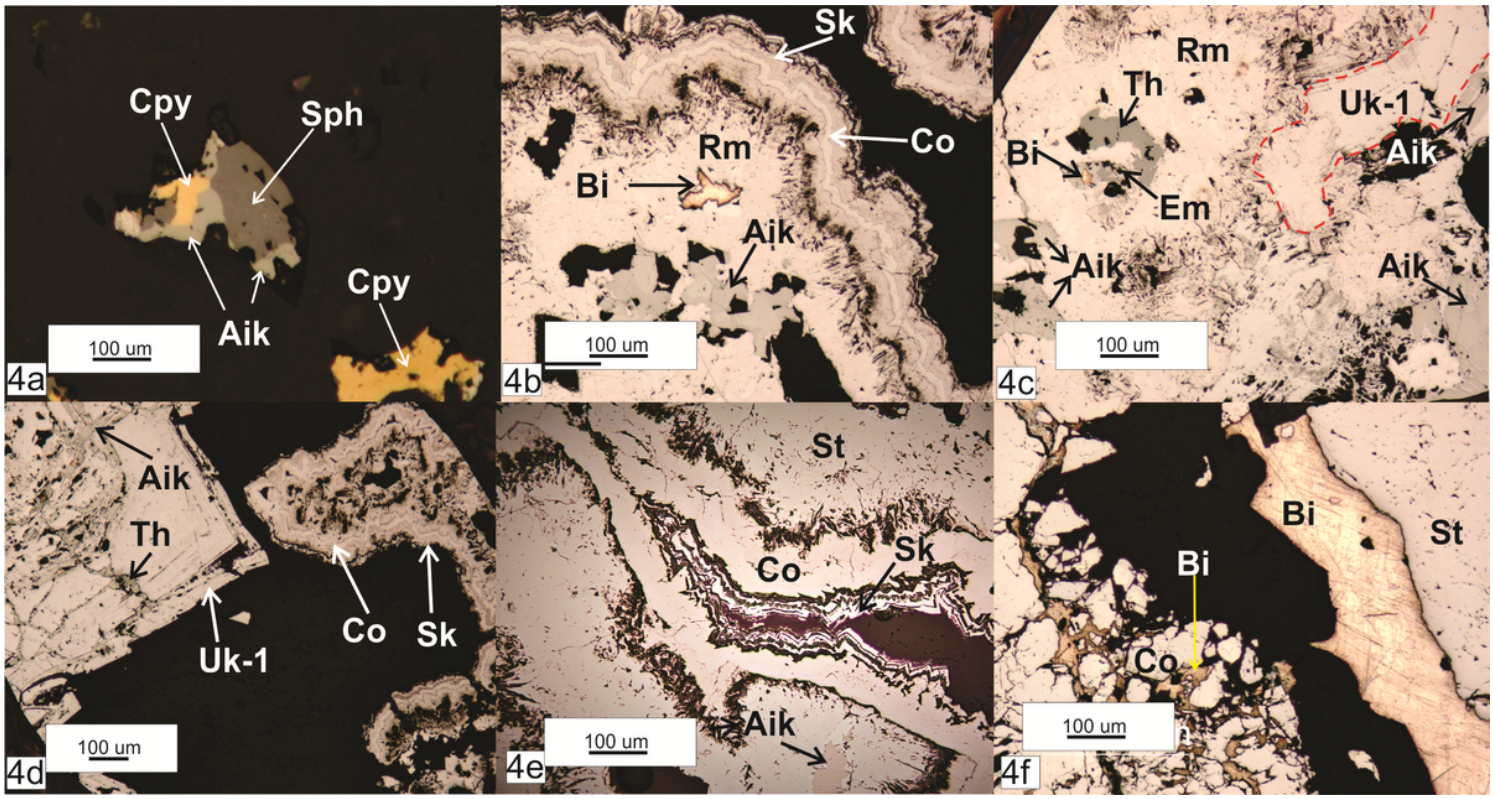

Figure 4

a) Aikinite rims sphalerite and chalcopyrite. b) Spherulitic rammelsbergite with inclusions of native bismuth and aikinite rimmed by cobaltite- skutterudite. c) Rammelsbergite with inclusions of tetrahedrite, aikinite, emplectite, native bismuth, and unknown 1. d) Aikinite filling cracks and growth zones in skutterudite. e) Safflorite rimmed by cobaltite and skutterudite. f) Native bismuth rims safflorite and fills cracks in cobaltite.

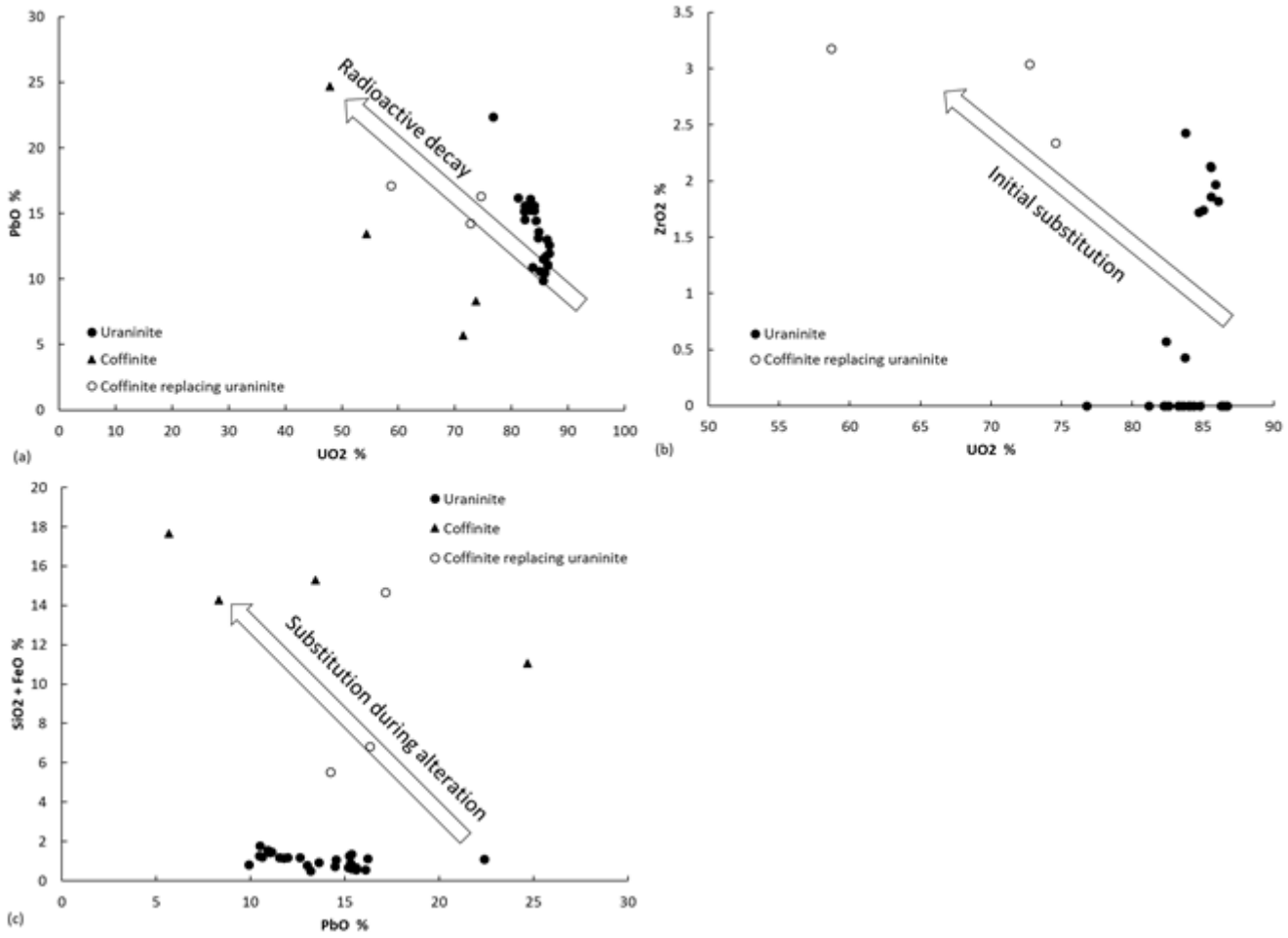

Figure 5

Plots showing effects of radioactive decay, initial substitution, and alteration on the composition of the Port Radium uraninite.

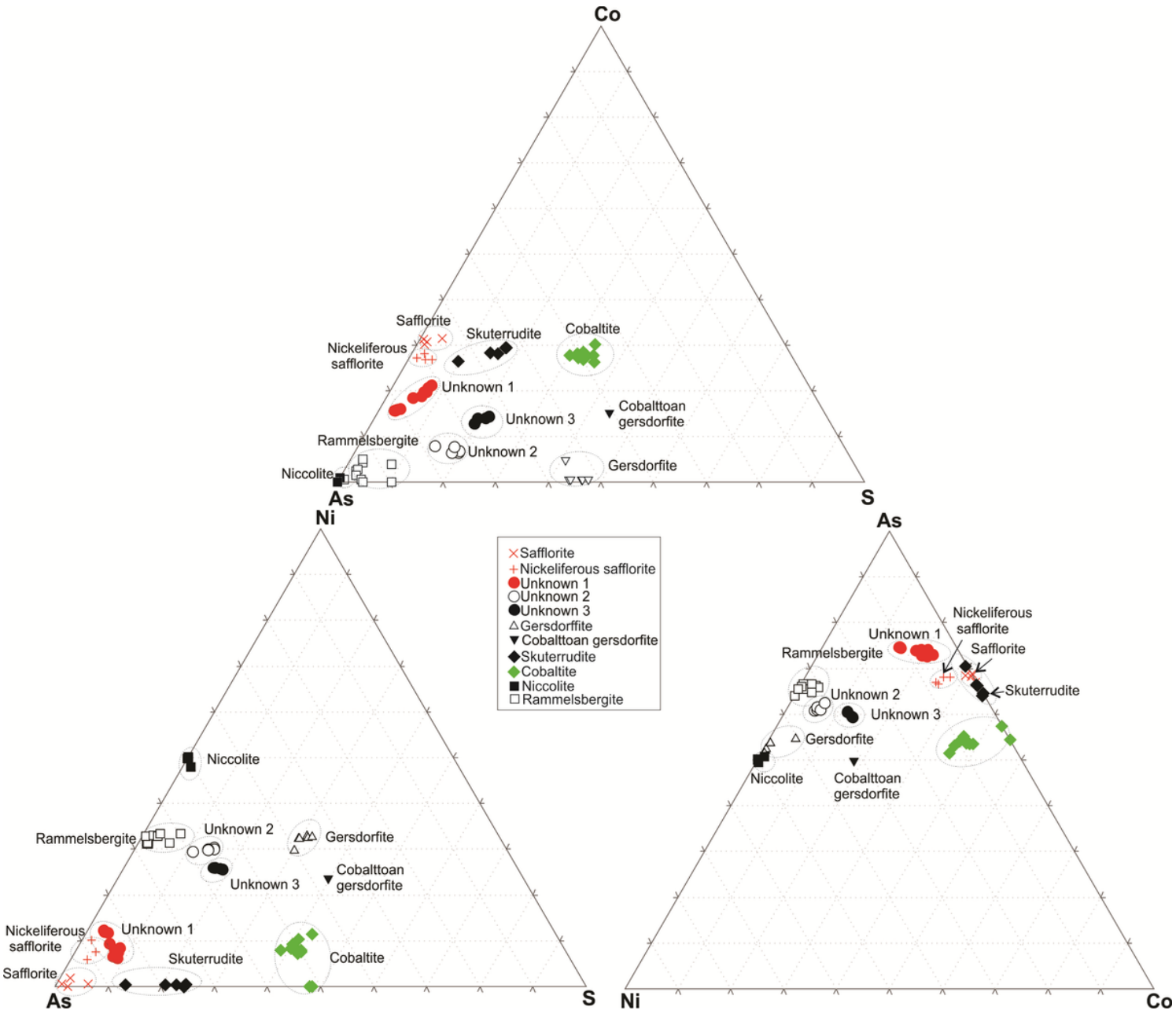

Figure 6

The Port Radium sulfarsenides in the Co-As-S, Ni-As-S, and As-Ni-Co diagrams showing discrete composition of three unknown minerals. Data plotted based on atoms per formula unit (apfu).

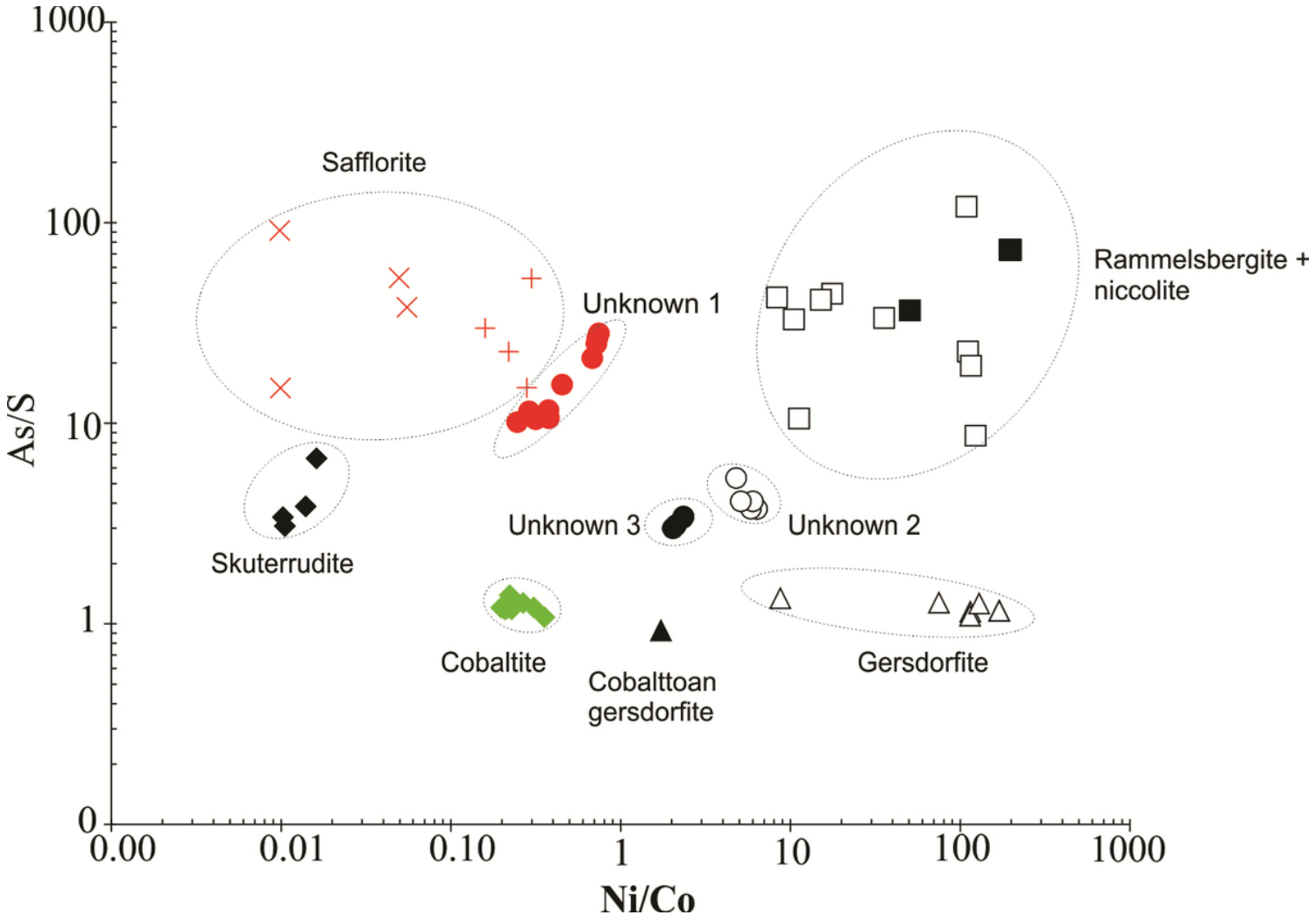

Figure 7

As/S vs. Ni/Co plot showing composition of the Port Radium sulfarsenides. The unknown minerals plot in the central part of the graph. Ratios are calculated using apfu.

Supplementary Files

This is a list of supplementary files associated with this preprint. Click to download.

- 3PortRadiumMineralogyPaperTables.doc